Molecular Cancer Therapeutics

Acetazolamide Serves as Selective Delivery Vehicle for Dipeptide-Linked Drugs to Renal Cell Carcinoma

Samuele Cazzamalli, Alberto Dal Corso, and Dario Neri

Abstract

In most cases, cytotoxic drugs do not preferentially accumulate at the tumor site, causing unwanted toxicities and preventing dose escalation to therapeutically active regimens. Here, we show that acetazolamide derivatives, which bind to carbonic anhydrase IX (CAIX) on the surface of kidney cancer cells, selectively deliver payloads at the site of disease, sparing normal organs. Biodistribution studies, performed in tumor-bearing mice with acetazolamide derivatives bearing a technetium-99m chelator complex or a red fluorophore as payload, revealed a preferential tumor accumulation of the compound at doses up to 560 nmol/kg. The percentage of injected dose per gram in the tumor was dose-dependent and revealed optimal tumor:organ ratios at 140 nmol/kg, with a tumor:blood ratio of 80:1 at 6 hours. Acetazolamide, coupled to potent cytotoxic drugs via a dipeptide linker, exhibited a potent antitumor activity in nude mice bearing SKRC-52 renal cell carcinomas, whereas drug derivatives devoid of the acetazolamide moiety did not exhibit any detectable anticancer activity at the same doses. The observation of tumor regression with a noninternalizing ligand and with different cytotoxic moieties (MMAE and PNU-159682) indicates a general mechanism of action, based on the selective accumulation of the product on tumor cells, followed by the extracellular proteolytic release of the cytotoxic payload at the neoplastic site and the subsequent drug internalization into tumor cells. Acetazolamide-based drug conjugates may represent a promising class of targeted agents for the treatment of metastatic kidney cancer, as the majority of human clear cell renal cell carcinomas are strongly positive for CAIX. *Mol Cancer Ther; 15(12); 2926–35. ©2016 AACR.*

Introduction

The majority of cytotoxic agents used for the pharmacotherapy of cancer do not preferentially accumulate at the tumor site, leading to potential toxicities and to suboptimal therapeutic efficacy (1–4). In tumor-bearing mice, unfavorable tumor:organ ratios have been reported for many drugs, including doxorubicin (5), paclitaxel (6), cisplatin (7), cyclophosphamide (8), sunitinib (9), and different fluorinated pyrimidines (10), to name just a few. For example, the relative uptake of doxorubicin in the tumor (expressed as percentage injected dose per gram or %ID/g) was found to be only 5% to 10% of the corresponding values in lung, heart, or liver, in the time period 0.5 to 8 hours (5). Importantly, similar trends are emerging from the positron emission tomography study of patients with cancer, who had received radiolabeled preparations of cytotoxic drugs (3, 4).

The coupling of potent cytotoxic payloads to antibodies or small organic molecules, acting as selective pharmacodelivery vehicles, has been proposed as a general strategy to improve the therapeutic index of anticancer drugs. Indeed, certain antibody–drug conjugates (ADCs; refs. 11–14) and small molecule–drug conjugates (SMDCs; ref. 2) have exhibited promising activity in preclinical models of cancer. Recently, 2 ADC products (Adcetris and Kadcyla) have gained marketing authorization for oncological applications.

Some ADCs cured tumors in mice at doses of 0.5 to 3 mg/kg, whereas the same products could be administered at 60-fold greater dose with acceptable safety profiles (15). Unfortunately, such a high therapeutic index is rarely observed in the clinic, suggesting that the tumor-targeting properties of the antibody, the drug release process, and/or the intrinsic sensitivity of tumor cells may be dramatically different in preclinical models and in patients with cancer. Nuclear medicine studies with radiolabeled antibody preparations have previously shown that lower tumor:organ ratios are often observed in humans compared with tumor-bearing mice, possibly reflecting differences in antigen abundance and vascular permeability (16, 17). SMDCs may represent an attractive alternative to ADC products, as smaller pharmaceuticals extravasate more rapidly and diffuse more homogenously within the neoplastic mass (2, 18–22). Unlike antibodies (which can easily be raised against the majority of target proteins of interest), it is not always easy to generate high-affinity small-molecule ligands to tumor-associated antigens. However, excellent tumor-targeting results have been reported for folate analogues targeting folate receptor–positive tumors (23, 24), substituted urea derivatives targeting prostate-specific membrane antigen (25), somatostatin antagonists targeting the somatostatin receptor (26) and for carbonic anhydrase IX (CAIX) ligands (16–18, 27).

It has generally been assumed that ADC and SMDC products would crucially rely on the use of ligands, capable of selective

Department of Chemistry and Applied Biosciences, Swiss Federal Institute of Technology (ETH Zürich), Zürich (Switzerland).

Note: Supplementary data for this article are available at Molecular Cancer Therapeutics Online (http://mct.aacrjournals.org/).

Corresponding Author: Dario Neri, Swiss Federal Institute of Technology (ETH Zürich), Vladimir-Prelog-Weg 1-5/10, Zürich 8093, Switzerland. Phone: 41-44-6337401; Fax: 41-44-6331358; E-mail: neri@pharma.ethz.ch

doi: 10.1158/1535-7163.MCT-16-0283

internalization of the conjugate into the tumor cells, followed by an intracellular liberation of the cytotoxic payload (11–14). This concept, however, has recently been challenged, as potent and selective anticancer activity has been observed with ADCs and SMDCs specific to antigens, which do not internalize (19, 20, 28–31).

CAIX is a membrane protein, expressed in the majority of clear cell renal cell carcinomas (32–34). CAIX is virtually undetectable in most normal adult tissues, except for certain structures in the gastrointestinal tract (stomach, duodenum, gallbladder), which are strongly positive for the antigen. Anti-CAIX monoclonal antibodies efficiently localize to metastatic renal cell carcinoma lesions in patients but, surprisingly, not to CAIX-positive stomach, duodenum, and gallbladder (35), suggesting that differences in vascular permeability may account for the process.

To the best of our knowledge, CAIX is a tumor-associated target which does not internalize (19), even though at least one anti-CAIX ADC product has been studied in the clinic in patients with cancer (36). CAIX-positive tumors can be efficiently targeted using certain small aromatic sulfonamides (18–20, 33, 37), including acetazolamide.

We have previously reported that acetazolamide can be used to deliver disulfide-linked derivatives of DM1 (a potent cytotoxic maytansinoid) to CAIX-positive tumors, leading to a potent antitumor effect (19, 20). We hypothesized that the extracellular drug release process at the tumor site would be facilitated by the death of tumor cells and the subsequent release of glutathione into the tumor extracellular space, which can work as a reducing agent on disulfide bonds, favoring an amplified cascade of drug release and tumor cell death. Since disulfide bonds can be unstable *in vivo* and since most anticancer drugs (unlike DM1) do not contain thiol groups suitable for coupling purposes, it would be interesting to learn whether potent noninternalizing SMDCs can be generated with stable peptidic linkers and with other classes of drugs. In this article, we describe that potent anticancer SMDCs can be generated by coupling acetazolamide to highly cytotoxic drugs (e.g., MMAE and PNU-159682), using a linker containing a valine–citrulline moiety and a self-immolative spacer. These findings reinforce the concept that potent antitumoral activity can be generated by the efficient release of toxic payloads in the tumor extracellular space, without ligand internalization into the target cells of interest.

Materials and Methods

Detailed synthetic procedures and characterization of the presented compounds (i.e., HPLC purity of final products, MS and NMR data, SPR assays) are described in the Supplementary Information (Supplementary Figs. S1–S11), together with additional biological data (i.e., stability of **4a** in the presence of Cathepsin B and CAIX, biodistribution in CAIX-negative lesions), and protocols (i.e., expression and purification of recombinant human CAIX; Supplementary Figs. S12–S15).

Peptide synthesis

Peptidic precursors of compounds **1–5** (Fig. 1) were synthesized by solid phase peptide synthesis (SPPS), using Fmoc-protected amino acids. Chlorotrityl resin (500 mg), preloaded with Fmoc-Cys(Trt)-OH, was swollen with DMF (10 ml) for 15 minutes inside a syringe equipped with a filter pad. Fmoc deprotection was achieved by shaking the resin with 20% v/v piperidine in DMF (5 mL) for 10 minutes for 3 times. After deprotection, the resin was washed with DMF (4 × 10 mL). Fmoc-protected amino acids (3 eq) were activated with HATU (3 eq) and DIPEA (6 eq) in DMF (5 mL) for 15 minutes in ice bath. After this time, the solution was allowed to react with the syringe for 1 hour and discarded and the resin washed with DMF (4 × 10 mL). Coupling and deprotection steps were alternated, to obtain the desired peptide sequence.

Acetazolamide or free amide moieties were then introduced by performing a CuAAC "click" reaction (38) with the corresponding peptide derivatives (carrying an azide moiety) on solid phase, followed by side chain deprotection, cleavage from the resin, and RP-HPLC purification.

Radiolabeling

Radiolabeling procedures with technetium-99m were performed essentially as described (18). Briefly, compound **1** (60 nmol) in TBS pH 7.4 (50 μL) was mixed with $SnCl_2$ (Sigma Aldrich, 200 μg) and sodium glucoheptonate (TCI, 20 mg) in H_2O (150 μL). TBS at pH 7.4 (600 μL) was added and the resulting solution degassed for 5 minutes by bubbling with nitrogen gas. The eluate from a ^{99m}Tc-generator (200 μL, ca. 200 MBq, Mallinckrodt) was added and the reaction mixture heated to 90°C for 20 minutes. After cooling to room temperature, an aliquot was analyzed by RP-HPLC (XTerra C18, 5% MeCN in 0.1% aq. TFA to 80% over 20 minutes on a Merck-Hitachi D-7000 HPLC system equipped with a Raytest Gabi Star radiodetector). Technetium-99m incorporations >95% were routinely achieved. The radioactive solution was then diluted to the desired concentrations with a molar excess of compound **1**, dissolved in TBS, pH 7.4.

Conjugates preparation

Peptide precursors of compounds **2–5** were dissolved in PBS (50 mmol/L phosphate, 100 mmol/L NaCl, pH 7.4) and a solution of maleimidocaproyl-linker-*p*-aminobenzylalcohol-drug in DMF was added at suitable molar ratios. The mixtures were stirred at room temperature until completion and the solvents were removed under vacuum. The conjugates were purified from the crude material via RP-HPLC and lyophilized to obtain the solid products. Purity was checked by UPLC on a Waters Acquity UPLC H-Class System using a ACQUITY UPLC BEH C18 Column, 130 Å, 1.7 μm, 2.1 mm × 50 mm column. Purities higher than 95% were routinely achieved. Details related to specific conjugates are reported in the Supplementary Information.

Cell cultures

The human renal cell carcinoma cell line SKRC-52 was kindly provided by Professor E. Oosterwijk in 2008 (Radboud University Nijmegen Medical Centre, Nijmegen, The Netherlands) and subsequently stored in liquid nitrogen. Upon thawing, cells were kept in culture for no longer than 14 passages, tested for CAIX expression by immunofluorescence, and not further authenticated. SKRC-52 and HEK293 (ATCC, CRL-1573) were maintained in RPMI medium (Invitrogen) supplemented with 10%, FCS (Invitrogen) and antibiotic/antimycotic (1%, AA, Invitrogen) at 37°C and 5% CO_2. For passaging, cells were detached using Trypsin-EDTA 0.05% (Invitrogen) when reaching 90% confluence and reseeded at a dilution of 1:6.

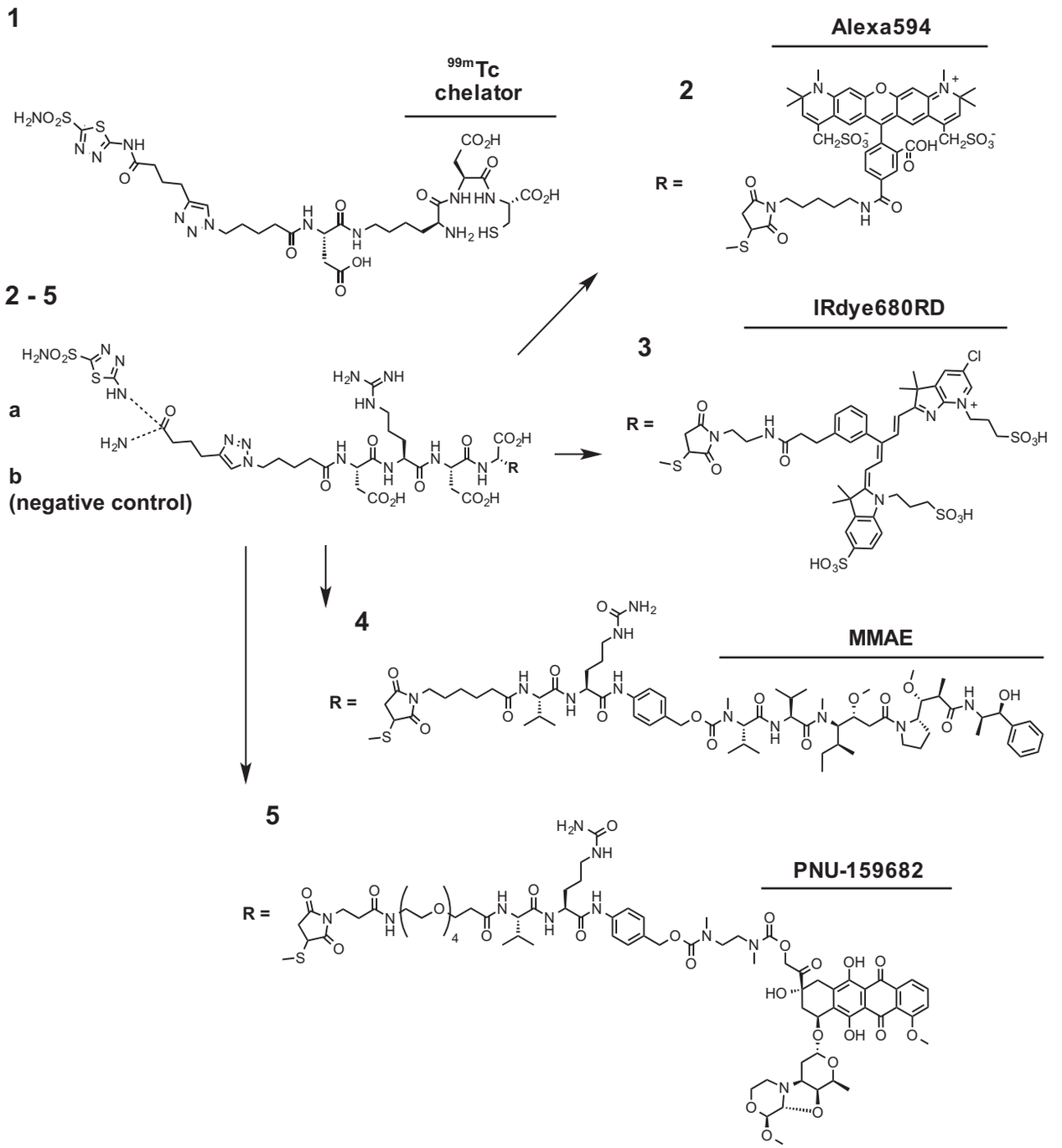

Figure 1.

Chemical structures of CAIX-targeting acetazolamide derivatives. Compound **1** features a ^{99m}Tc-chelating moiety, whereas compounds **2a** and **3a** contain, respectively, an Alexa594 or a IRdye680RD fluorophore moiety. Cytotoxic drug derivatives featured an acetazolamide moiety (**a** series) or an amide (**b** series, serving as negative control). Products containing the MMAE (compounds **4a** and **4b**) or PNU-159682 payload (compounds **5a** and **5b**) featured a Asp-Arg-Asp-Cys spacer, a valine–citrulline dipeptide cleavable linker, as well as a self-immolative linker.

Ligand internalization analysis by confocal microscopy

SKRC52 or HEK 293 cells were seeded into 4-well coverslip chamber plates (Sarstedt) at a density of 10^4 cells per well in RPMI medium (1 mL, Invitrogen) supplemented with 10% FCS, AA, and HEPES (10 mmol/L) and allowed to grow for 24 hours under standard culture conditions. The medium was replaced with medium containing **2a** or **2b** (120 nmol/L), after 30 minutes or 1 hour, Hoechst 33342 nuclear dye (Invitrogen) was added and

randomly selected cells imaged on an SP8 confocal microscope equipped with an AOBS device (Leica Microsystems).

Linker stability assays

Compounds **4a** and **5a** were dissolved in PBS (100 μg/mL) and incubated at 37°C in a shaking incubator. Aliquots (150 μL) were taken at different time points (0 minutes, 15 minutes, 1, 6, 24, 48 hours) and frozen at −20°C. Standard solutions of the conjugates were prepared in PBS at different concentration (25, 50, 100, 150 μg/mL) and stored at −20°C. The standards and the samples were analyzed in triplicate by liquid chromatography/mass spectrometry (LC-MS) on a Waters Xevo G2-XS QTOF coupled to a Waters Acquity UPLC H-Class System using a ACQUITY UPLC BEH C18 Column, 130 Å, 1.7 μm, 2.1 mm × 50 mm column. Peaks relative to the intact SMDCs were integrated, and area values from the standards were used to obtain calibration curves. Concentration of intact test compounds in the samples was determined at the different time points to obtain a stability profile of the conjugates.

To measure mouse serum stabilities of the conjugates, the compounds were dissolved in freshly thawed mouse serum (Invitrogen; 100 μg/mL) and incubated at 37°C in a shaking incubator. Aliquots of 150 μL were taken at different time points (0, 20 minutes, 1, 3, 6, 24 hours) and frozen at −20°C. Standard solutions were prepared in mouse serum (Invitrogen) at different concentration (25, 50, 100, 150 μg/mL) and stored at −20°C. All the samples and the standards were thawed and diluted with 4 volumes of MeOH. After vigorous vortex agitation for 1 minute, the protein precipitate was spun down and 400 μL of the supernatant were lyophilized overnight. The resulting solid material was re-dissolved in 100 μL of Millipore water and analyzed as described above.

In vitro cytotoxicity assay

SKRC-52 cells were seeded in 96-well plates in RPMI added with 10% FCS (100 μL) at a density of 5,000 cells per well and allowed to grow for 24 hours. The medium was replaced with medium containing different concentrations of test substance (1:3 dilution steps) and plates were incubated under standard culture conditions. After 72 hours, the medium was removed, MTS cell viability dye (20 μL, Promega) in 150 μL of the medium was added, the plates were incubated for 2 hours under culture conditions, and the absorbance at 490 nm measured on a Spectra Max Paradigm multimode plate reader (Molecular Devices). Experiments were performed in triplicate and average cell viability calculated as measured background corrected absorbance divided by the absorbance of untreated control wells. IC_{50} values were determined by fitting data to the 4-parameter logistic equation, using a Prism 6 software (GraphPad Software) for data analysis.

Animal studies

All animal experiments were conducted in accordance with Swiss animal welfare laws and regulations under the license number 27/2015 granted by the Veterinäramt des Kantons Zürich.

Implantation of subcutaneous SKRC-52 tumors

SKRC-52 cells were grown to 80% confluence and detached with Trypsin-EDTA 0.05% (Life Technologies). Cells were washed with Hank balanced salt solution (HBSS, pH 7.4) once, counted and resuspended in HBSS to a final concentration of 3.4×10^7 cells/mL. Aliquots of 5×10^6 cells (150 μL of a suspension) were injected subcutaneously in the right flank of female athymic Balb/c *nu/nu* mice (8–10 weeks of age, Janvier).

Quantitative biodistribution studies

SKRC-52 xenografted tumors were implanted into female Balb/c *nu/nu* mice (Janvier) as described above and allowed to grow for 3 weeks to an average volume of 0.25 mL. Mice were randomized ($n = 5$ per group) and injected intravenously with different doses of radiolabelled preparations (15–25 MBq, 70–560 nmol/kg). Mice were sacrificed 6 hours after the injection by CO_2 asphyxiation and organs extracted, weighted, and radioactivity measured with a Packard Cobra γ-counter. Values are expressed as %ID/g ± SD.

IVIS imaging

Female Balb/c *nu/nu* mice bearing subcutaneous SKRC-52 tumors were injected intravenously with Compound **3a**, containing the near-infrared dye moiety IRDye680RD (LI-COR Biosciences; 250 nmol/kg), dissolved in sterile PBS (100 μL). Mice were anesthetized with isoflurane and fluorescence images acquired on an IVIS Spectrum imaging system (Xenogen, exposure 1 second, binning factor 8, excitation at 675 nm, emission filter at 720 nm, f number 2, field of view 13.1). Images were taken before the injection and after 10 minutes, 1, 3, and 6 hours. Food and water was given *ad libitum* during that period.

Dose escalation study

Recommended dose of compound **4a** suitable for therapy experiments was determined by dose escalation in wild-type female athymic Balb/c *nu/nu* mice (8–10 weeks of age, Janvier). A schedule of 5 injections on 5 consecutive days was used to compare increasing doses (250 or 500 nmol/kg) of the targeted derivative **4a** with untargeted compound **4b** (Supplementary Fig. S13). Three mice were used for each group. Tolerated dose was defined when animals did not lose more than 5% of their initial body weight over the duration of the experiment after the initial injection.

Therapy experiments

SKRC-52 xenografted tumors were implanted into female Balb/c *nu/nu* mice (Janvier) as described above and allowed to grow for 2 weeks to an average volume of 0.1 mL. Mice were randomly assigned into therapy groups of 4 or 5 animals and treatment started by injecting a solution of the targeted drugs, untargeted drugs, or vehicle (PBS only or PBS containing 1% of DMSO) intravenously (tail vein) at the doses and with the schedules indicated in the text. Compounds **4a** and **4b** were injected as solutions in sterile PBS. Compounds **5a** and **5b** were injected as solutions in sterile PBS containing 1% DMSO. Animals were weighed and tumor sizes measured daily with an electronic caliper. The tumor volume was calculated according to the formula: (long side) × (short side) × (short side) × 0.5. Animals were sacrificed when the termination criteria were reached. Prism 6 software (GraphPad Software) was used for data analysis (regular 2-way ANOVA with the Bonferroni test).

Immunofluorescence studies

SKRC-52 tumors were excised from the animals treated with conjugate **5a** or alternatively with vehicle during the therapy experiment, embedded in OCT medium (Thermo Scientific), and cryostat sections (10 μm) were cut. Slides were stained using the

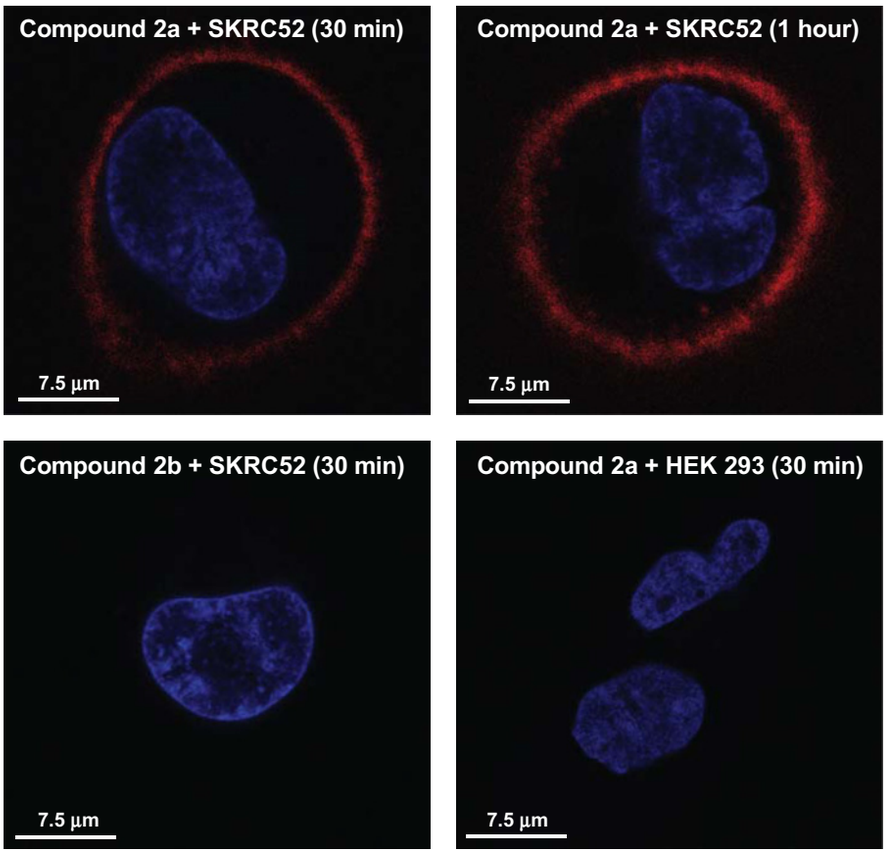

Figure 2.
Confocal microscopy image of CAIX-expressing SKRC-52 cells after exposure to targeted dye conjugate **2a** (120 nmol/L) at different incubation times. The conjugate is mainly bound to the cell surface. Alternatively SKRC-52 cells were exposed to untargeted dye conjugate **2b** (120 nmol/L) for 30 minutes. CAIX-negative HEK 293 cells were also exposed to targeted dye conjugate **2a** (120 nmol/L) for 30 minutes. No cell surface binding can be detected for both the negative controls. Red = Alexa594 derivatives staining; Blue = Hoechst 33342 staining.

following antibodies: mouse anti-human CAIX GT12 (Thermo Scientific) to detect the antigen and rat anti-mouse CD31 (BD Biosciences) to detect endothelial cells. Nuclear staining was performed with DAPI. Anti-mouse IgG-AlexaFluor488 (Molecular Probes by Life Technologies) and anti-rat IgG-AlexaFluor594 (Molecular Probes by Life Technologies) were then used as secondary antibodies for microscopic detection.

Results

Synthesis and tumor-targeting properties of acetazolamide derivatives

Acetazolamide was coupled to a Lys-Asp-Cys–based ^{99m}Tc-chelating moiety, which had previously been used for the imaging of patients with cancer with folate derivatives (39), using a "click" chemistry reaction (Fig. 1). The resulting conjugate **1** could be labeled with ^{99m}Tc (radiolabel incorporation >95% routinely achieved; 160–210 MBq/mL) for quantitative biodistribution analysis in tumor-bearing mice. Click chemistry was also used to install the acetazolamide moiety onto Asp-Arg-Asp-Cys peptidic derivatives, which were subsequently coupled to a red Alexa fluorophore (Compound **2a**), a near-infrared dye (Compound **3a**), or cytotoxic drugs, based on the monomethyl auristatin E (MMAE; Compound **4a**) or PNU-159682 (Compound **5a**) active moieties (Fig. 1). As negative controls devoid of CAIX binding, derivatives containing an amide function instead of the acetazolamide moiety were used (Compounds **2b**, **4b**, and **5b**).

Confocal microscopy experiments were performed to investigate the internalization of our acetazolamide derivatives upon ligand binding to CAIX. SKRC-52 cancer cells (expressing high levels of CAIX) were incubated with compound **2a** and the fluorescence derived from Alexa594-labeled acetazolamide was imaged after incubation for 30 and 60 minutes (Fig. 2). Compound **2a** showed selective accumulation on the membrane SKRC-52 cells, as compared with CAIX-negative HEK 293 cells. No intracellular fluorescence was observed throughout the experiment, indicating that the AAZ binding to CAIX was not followed by a significant receptor-mediated endocytosis. In a control experiment, compound **2b**, devoid of the targeting moiety, showed no interaction with CAIX-positive SKRC-52 cells (Fig. 2).

The tumor-targeting properties of acetazolamide derivatives were characterized using both radioactive and near-infrared fluorescence methods in nude mice bearing subcutaneously grafted SKRC-52 tumors (40). Compound **1**, labeled with ^{99m}Tc, was injected intravenously at doses ranging between 70 and 560 nmol/kg. A preferential tumor uptake was observed 6 hours after intravenous administration at all doses (Fig. 3A). However, a progressive decrease in percent injected dose per gram of tumor was detected, reflecting target saturation at the highest dose. Interestingly, compound uptake in normal organs (e.g., liver, lung, kidney, intestine, stomach) also decreased at higher doses. These biodistribution results suggested that doses around 200 to 300 nmol/kg may represent a good compromise between high tumor uptake and low accumulation in normal tissues. The near-

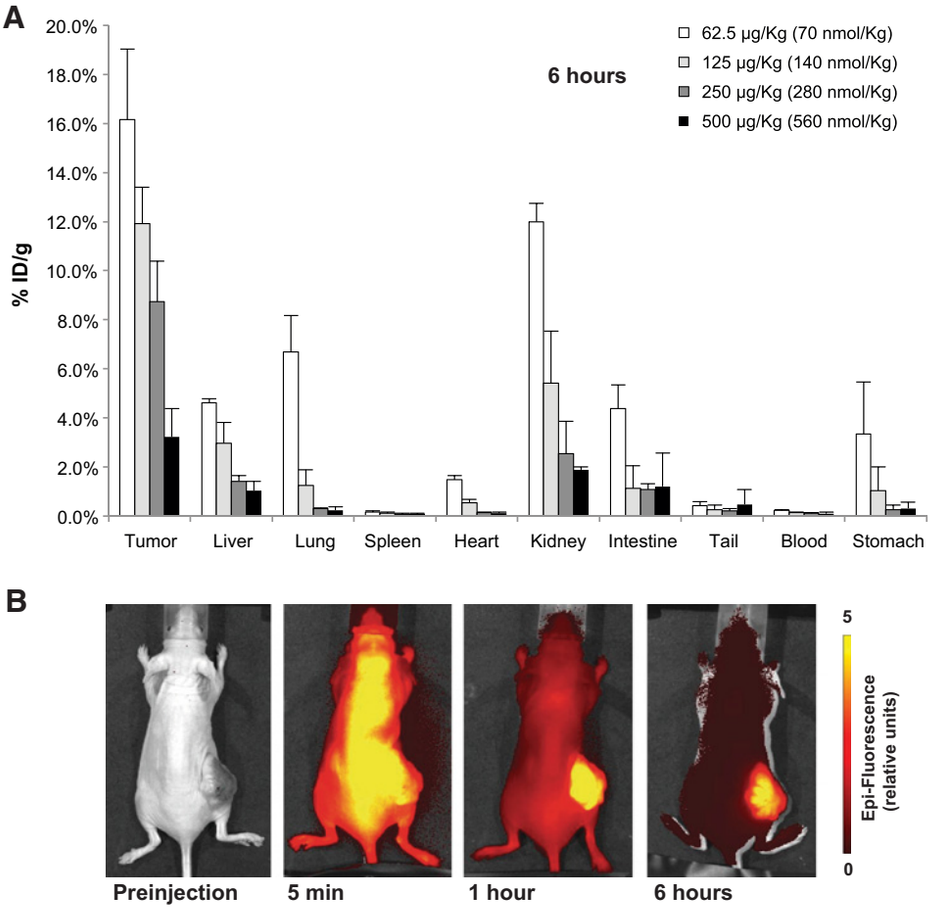

Figure 3.
A, Organ distribution of ^{99m}Tc radiolabeled compound **1** injected at different doses in Balb/c *nu/nu* mice bearing SKRC-52 xenografts ($n = 5$ per group). The data, expressed as mean %ID/g of tissue ± SD, correspond to the 6-hour time point after the intravenous administration of the radiolabeled compound. **B,** Near-infrared fluorescence imaging evaluation of the targeting performance of the IRDye680RD conjugate **3a** in Balb/c *nu/nu* mice bearing SKRC-52 xenografts.

infrared fluorescent derivative **3a**, administered at 250 nmol/kg, was shown to preferentially accumulate in the tumor at various time points, between 5 minutes and 6 hours (Fig. 3B). These results are in keeping with the ones previously reported by our group with similar fluorescently labeled derivatives (17, 18, 30), indicating that the acetazolamide moiety can deliver different types of payloads to SKRC-52–positive tumors.

Prior to therapy studies, the stability of acetazolamide-drug conjugates **4a** and **5a** was investigated *in vitro* at 37°C, both in PBS and in mouse serum (Fig. 4). For both compounds, a half-life in PBS >48 hours was observed. A lower stability was seen in mouse serum, but >70% of both conjugates were intact after 6 hours (i.e., a sufficiently long time, compared with the circulatory half-life of acetazolamide derivatives in blood, which is typically shorter than 15 minutes; ref. 16). Mass spectrometric analysis of compound **4a** revealed free MMAE as the main release product, whereas in the degradation profile of compound **5a** in mouse serum, free PNU-159682 was not identified, probably due to low sensitivity of the mass spectrometer to a such hydrophobic moiety.

An *in vitro* toxicity study, performed with SKRC-52 cells incubated with the conjugates **4a,b-5a,b** or with the corresponding unmodified drugs, confirmed that the acetazolamide coupling had led to the formation of prodrugs. Indeed, all the conjugates resulted to be less toxic compared with the parental cytotoxic moieties (Fig. 5).

Therapy experiments

Compounds **4a** and **5a** were used in therapy experiments with nude mice bearing subcutaneous SKRC-52 tumors. The maximum tolerated doses of the 2 prodrugs were determined by dose escalation experiments and found to be 500 nmol/kg for compound **4a** (Supplementary Fig. S13) and 50 nmol/kg for compound **5a**. The MMAE conjugate **4a**, used at a dose of 250 nmol/kg with 10 daily administrations, exhibited a potent antitumor activity effect (P <0.0001 at day 26, compared with the control groups), whereas compound **4b** (devoid of the acetazolamide moiety and serving as negative control) did not retard tumor growth (Fig. 6A). In these experimental conditions, no acute toxicity and no significant weight loss was observed for the group of mice treated with the acetazolamide–MMAE conjugate **4a** (Fig. 6B). One of 5 mice enjoyed a durable complete response (with no tumor regression for the next 4 months), whereas lesions started to regrow in the remaining 4 mice 1 week after the last injection.

The antitumor efficacy of the PNU-159682 conjugate **5a** was investigated at a dose of 25 nmol/kg (Fig. 6C). Also in this case, the conjugate **5a** exhibited a potent antitumor effect, whereas the negative control compound **5b** did not inhibit tumor growth, confirming the crucial role of the acetazolamide moiety for the potentiation of drug activity. An additional group of animals was injected with equimolar doses of compound **5a** and the acetazolamide derivative **3a**, leading to a slight decrease in therapeutic activity and tolerability (Fig. 6C). The treatment of mice with

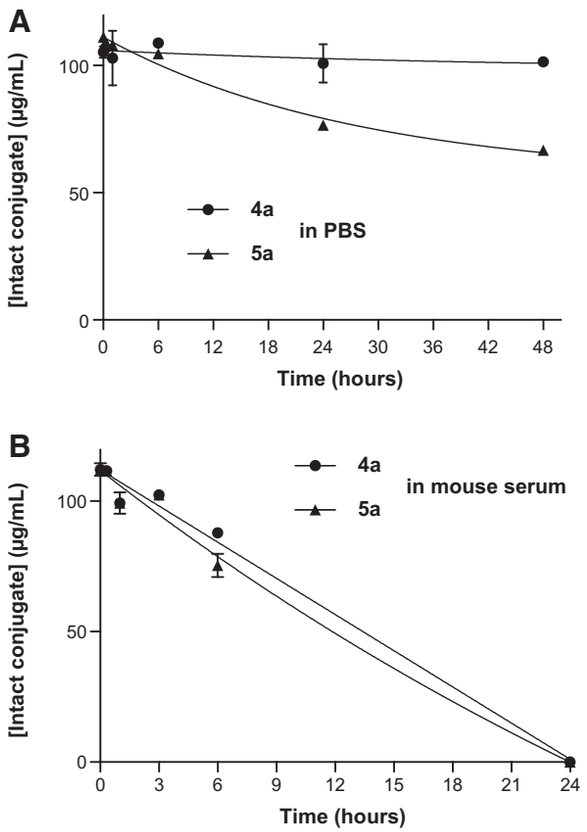

Figure 4.

Stability of prodrugs **4a** and **5a** in PBS, pH 7.4 (**A**), and in mouse serum (**B**) at 37°C as determined by LC-MS. Dipeptide derivatives of both types of payload were found to be highly stable in saline solution ($t_{1/2}$ >48 hours). A lower stability was observed in mouse serum, but at least 70% of the compounds were still intact after 6 hours of incubation.

PNU-159682 derivatives was associated with higher toxicity compared with the results obtained with MMAE conjugates, but the **5a** treatment group completely recovered from a reversible 10% body weight loss (Fig. 6D). At day 40, a second therapeutic cycle of 4 injections was performed, which did not lead to the disappearance of neoplastic lesions. To investigate the reasons for the absence of therapeutic activity in the second treatment cycle, mice were injected with the fluorescently labeled acetazolamide derivative **3a** (250 nmol/kg) which exhibited only a faint tumor accumulation (Fig. 7A), in stark contrast to predosing results (Fig. 3B). An immunofluorescence analysis of resected tumors confirmed that cancer cells remained strongly positive for CAIX (Fig. 7B), suggesting that a reduction in vascular permeability after therapy may have impaired drug accumulation in the neoplastic lesions.

Discussion

Acetazolamide derivatives selectively localize to renal cell carcinoma xenografts in mice, which express CAIX as membrane protein. The interaction of these compounds with CAIX-expressing cells has been investigated at the cellular level, by means of fluorescence microscopy experiments. The latter showed that acetazolamide-bearing conjugates bind to CAIX on the cell membrane without triggering a receptor-mediated endocytosis, in agreement with previous findings (19, 20).

A pool of AAZ-based SMDCs has been prepared by our group in recent years: different types of cytotoxic drugs (DM1, MMAE, or PNU-159682) were attached to acetazolamide via cleavable linkers (i.e., disulfide bond or valine–citrulline peptide). These SMDCs were found to have similar serum half-lives, which were sufficiently high to exhibit therapeutic benefits *in vivo*. In particular, the new valine–citrulline–bearing compounds **4a** and **5a** exhibited a half-life of about 7 hours in serum, which is substantially longer than the circulatory half-life of the radiolabeled analogue **1**.

While drugs commonly used for the treatment of metastatic kidney cancer (e.g., sorafenib and sunitinib) did not display any detectable activity against SKRC-52 tumors (20), acetazolamide derivatives of MMAE (a tubulin inhibitor) and of PNU-159682 (a nemorubicin metabolite) could suppress tumor growth, sometimes mediating a complete tumor eradication. The removal of the acetazolamide moiety from the linker–payload combinations

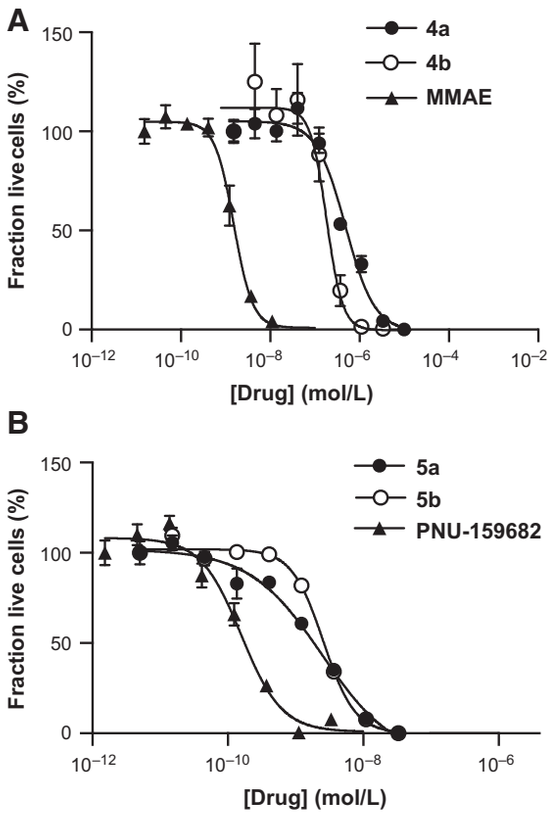

Figure 5.

Toxicity of (**A**) MMAE derivatives **3a** and **3b**, (**B**) PNU-159682 derivatives **4a** and **4b** and the corresponding unmodified payloads toward CAIX-expressing SKRC-52 cells. Cells were incubated for 72 hours in the presence of various concentrations of the test compound at 37°C. Data points are averages of 3 experiments. Error bars indicate SDs. Cytotoxicity values for targeted and nontargeted conjugates are comparable in these *in vitro* experiments (IC_{50} values: 485 nmol/L for **4a**, 204 nmol/L for **4b**, 25 nmol/L for **5a**, 26 nmol/L for **5b**), confirming the absence of efficient internalization. In all cases, prodrugs were found to be less potent *in vitro* than the parental free cytotoxic compound (IC_{50} values: 1.5 nmol/L for MMAE, 0.16 nmol/L for PNU-159682).

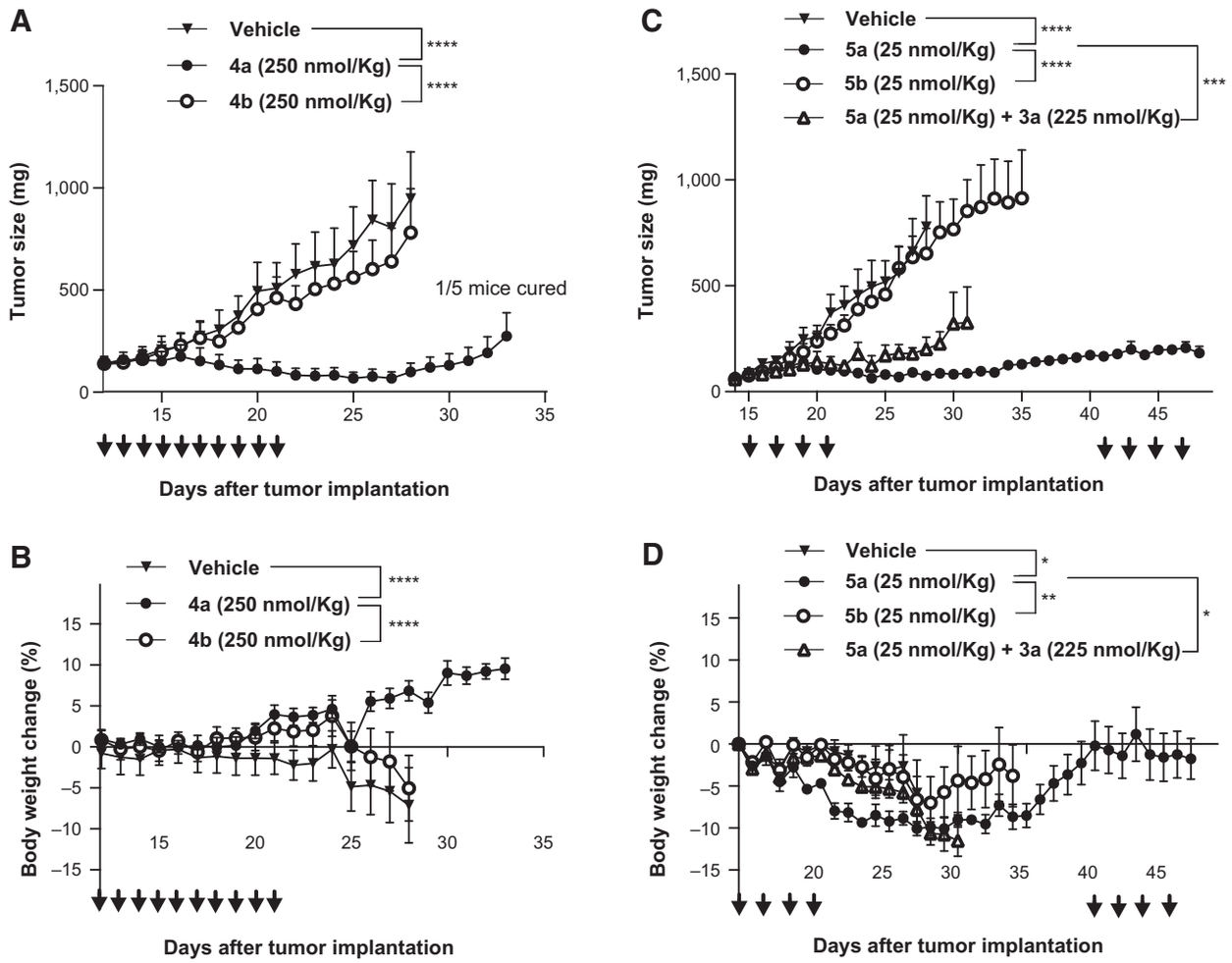

Figure 6.

Therapeutic activity of compound **4a** (**A**; 250 nmol/kg) and **5a** (**C**; 25 nmol/kg) in Balb/c *nu/nu* mice bearing SKRC-52 xenografts. In the experiments, drug derivatives devoid of the acetazolamide moiety were used as negative controls (**4b** and **5b**). The graphs in (**B**) and (**D**) show the changes in body weight for the treated animals. The statistical analysis of the therapy results, comparing the therapeutic outcome with acetazolamide derivatives and the data obtained with **4b** and **5b** compounds, indicate superior efficacy of the acetazolamide-based conjugates. ****, $P < 0.0001$; ***, $P < 0.001$; **, $P < 0.01$; *, $P < 0.05$.

abrogated therapeutic activity in all experimental systems, confirming that the ligand-based delivery of cytotoxic drugs to the extracellular tumor environment represents a strict requirement for anticancer efficacy. Both compounds **4a** and **5a** described in this article feature a linker containing a valine–citrulline moiety, which was previously believed to be particularly suited for the intracellular release of drug payloads, due to the action of lysosomal cathepsin B (41). This protein is a primarily intracellular protease that can be secreted extracellularly by dying cells but also by living tumor cells to initiate extracellular proteolytic cascades and to enable tumor cell proliferation (42). Our therapy data suggest that the presence of cathepsin B in the extracellular tumor environment is sufficient for the efficient liberation of cytotoxic drug moieties, which can then diffuse into surrounding tumor cells.

Nude mice do not represent a perfect model for the assessment of anticancer agents for a number of reasons (43), including their lack of T cells. It has recently been shown that certain cytotoxic agents can mediate an immunogenic tumor cell death (44, 45). In addition, certain immunostimulatory agents (e.g., antibody–cytokine fusion proteins, immunologic checkpoint inhibitors) may potently synergize with some cytotoxic agents (46–48).

Despite the fact that a strong suppression of tumor growth was observed both for compounds **4a** and **5a**, cancer cures were rare. Interestingly, treatment of mice with a second cycle of **5a** therapy did not cause a second tumor regression (Fig. 6). Macroscopic and microscopic imaging data suggest that the tumor uptake of acetazolamide derivatives is reduced after therapy, probably as a result of changes in vascular permeability at the neoplastic site, whereas cancer cells remain CAIX-positive. It will be interesting to investigate whether similar findings can be observed with other classes of targeted cytotoxics (e.g., with ADC products).

The potent therapeutic activity observed with compounds **4a** and **5a** suggests that these products may provide a benefit to

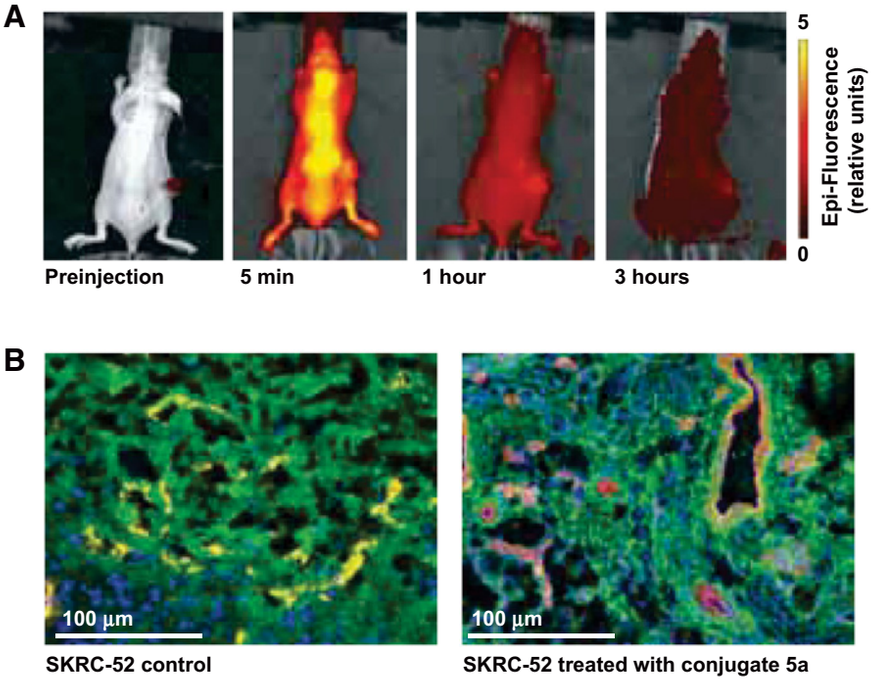

Figure 7.
Analysis of tumor targeting after therapy experiments. **A,** Imaging of a mouse, carrying a subcutaneously grafted SKRC-52 tumor, with 250 nmol/kg of the fluorescent acetazolamide derivative **3a**, performed 34 days after the beginning of therapy with compound **5a**. A striking difference in tumor uptake compared with the data of Fig. 2B can be observed. **B,** Microscopic analysis of representative sections of SKRC-52 tumors, before and after therapy with the acetazolamide derivative **5a**. Green = CAIX staining; Red = CD31 staining; Yellow = overlap of the 2 colors; Blue = DAPI staining.

patients with kidney cancer, as the majority of clear cell renal cell carcinomas are strongly positive for this target (32–34). The biodistribution profiles of acetazolamide derivatives compares favorably with the ones previously reported for other ligands (23–26). In particular, we were pleased to see that %ID/g values in the tumor were higher than the corresponding values in the kidney (the main organ for drug clearance), even as early as 1 hour after intravenous administration of the product (18). A nuclear medicine trial in patients with metastatic renal cell carcinoma is currently planned for ^{99m}Tc-labeled acetazolamide **1**. That study will provide essential information, regarding the tumor:organ ratios that can be expected in patients with cancer and in mouse models of the disease.

Disclosure of Potential Conflicts of Interest

D.N. is a board member of, reports receiving a commercial research grant from, has ownership (including patents) in, and is a consultant/advisory board member for Philogen. No potential conflicts of interest were disclosed by the other authors.

Authors' Contributions

Conception and design: S. Cazzamalli, D. Neri
Development of methodology: S. Cazzamalli, A. Dal Corso, D. Neri
Acquisition of data (provided animals, acquired and managed patients, provided facilities, etc.): S. Cazzamalli, A. Dal Corso
Analysis and interpretation of data (e.g., statistical analysis, biostatistics, computational analysis): S. Cazzamalli, A. Dal Corso, D. Neri
Writing, review, and/or revision of the manuscript: S. Cazzamalli, A. Dal Corso, D. Neri
Administrative, technical, or material support (i.e., reporting or organizing data, constructing databases): S. Cazzamalli, D. Neri
Study supervision: D. Neri

Acknowledgments

We thank Franziska Bootz, Rémy Gébleux, Dario Venetz, and Jonathan Kiefer for their help with experimental procedures. We also thank Alessandra Villa for CAIX production. The authors acknowledge support of the Scientific Center for Optical and Electron Microscopy ScopeM of the Swiss Federal Institute of Technology ETHZ. We personally acknowledge Justine Kusch for the help with confocal microscopy. Nikolaus Krall is acknowledged for many comments and suggestions.

Grant Support

D. Neri gratefully acknowledges ETH Zürich, the Swiss National Science Foundation (Projects Nr. 310030B_163479/1), ERC Advanced Grant "Zauberkugel," Kommission für Technologie und Innovation (Grant Nr. 17072.1), Bovena Foundation, and Maiores Foundation for financial support.

The costs of publication of this article were defrayed in part by the payment of page charges. This article must therefore be hereby marked *advertisement* in accordance with 18 U.S.C. Section 1734 solely to indicate this fact.

Received May 5, 2016; revised July 27, 2016; accepted August 28, 2016; published OnlineFirst September 8, 2016.

References

1. Krall N, Scheuermann J, Neri D. Small targeted cytotoxics: current state and promises from DNA-encoded chemical libraries. Angew Chem Int Ed Engl 2013;52:1384–402.
2. Srinivasarao M, Galliford CV, Low PS. Principles in the design of ligand-targeted cancer therapeutics and imaging agents. Nat Rev Drug Discov 2015;14:203–19.
3. Van der Veldt AAM, Hendrikse NH, Smit EF, Mooijer MPJ, Rijnders AY, Gerritsen WR, et al. Biodistribution and radiation dosimetry of C-11-labelled docetaxel in cancer patients. Eur J Nucl Med Mol Imaging 2010;37:1950–58.
4. Van der Veldt AAM, Lubberink M, Mathijssen RHJ, Loos WJ, Herder GJM, Greuter HN, et al. Toward prediction of efficacy of chemotherapy: a proof of

concept study in lung cancer patients using C-11 docetaxel and positron emission tomography. Clin Cancer Res 2013,19,4163–73.
5. Bosslet K, Straub R, Blumrich M, Czech J, Gerken M, Sperker B, et al. Elucidation of the mechanism enabling tumor selective prodrug monotherapy. Cancer Res 1998;58:1195–201.
6. Cao Q, Li ZB, Chen K, Wu Z, He L, Neamati N, et al. Evaluation of biodistribution and anti-tumor effect of a dimeric RGD peptide–paclitaxel conjugate in mice with breast cancer. Eur J Nucl Med Mol Imaging 2008;35:1489–98.
7. Oberoi HS, Nukolova NV, Laquer FC, Poluektova LY, Huang J, Alnouti Y, et al. Cisplatin-loaded core cross-linked micelles: comparative pharmacokinetics, antitumor activity, and toxicity in mice. Int J Nanomedicine 2012; 7:2557–71.
8. Kesner AL, Hsueh WA, Htet NL, Pio BS, Czernin J, Pegram MD, et al. Biodistribution and predictive value of ^{18}F-fluorocyclophosphamide in mice bearing human breast cancer xenografts. J Nucl Med 2007;48:2021–7.
9. Kuchar M, Oliveira MC, Gano L, Santos I, Kniess T. Radioiodinated sunitinib as a potential radiotracer for imaging angiogenesis—radiosynthesis and first radiopharmacological evaluation of 5-[^{125}I]Iodo-sunitinib. Bioorg Med Chem Lett 2012;22:2850–5.
10. Abe Y, Fukuda H, Ishiwata K, Yoshioka S, Yamada K, Endo S. Studies on ^{18}F-labeled pyrimidines. Tumor uptakes of 18F-5-fluorouracil 15F-5-fluorouridine, and 18F-5-fluorodeoxyuridine in animals. Eur J Nucl Med Mol Imaging 1983;8:258–61.
11. Senter PD. Potent antibody drug conjugates for cancer therapy. Curr Opin Chem Biol 2009;13:235–44.
12. Chari RVJ, Miller ML, Widdison WC. Antibody-drug conjugates: an emerging concept in cancer therapy. Angew Chem Int Ed Engl 2014;53: 3796–827.
13. Panowski S, Bhakta S, Raab H, Polakis P, Junutula JR. Site-specific antibody drug conjugates for cancer therapy. MAbs 2014;6:34–45.
14. Gerber HP, Koehnb FE, Abraham RT. The antibody-drug conjugate: an enabling modality for natural product-based cancer therapeutics. Nat Prod Rep 2013;30:625–39.
15. Doronina SO, Toki BE, Torgov MY, Mendelsohn BA, Cerveny CG, Chace DF, et al. Development of potent monoclonal antibody auristatin conjugates for cancer therapy. Nat Biotechnol 2003;21:778–84.
16. Poli GL, Bianchi C, Virotta G, Bettini A, Moretti R, Trachsel E, et al. Radretumab radioimmunotherapy in patients with brain metastasis: A ^{124}I-L19SIP Dosimetric PET Study. Cancer Immunol Res 2013;1:134–43.
17. Smaldone MC, Chend DY, Yu JQ, Plimack ER. Potential role of ^{124}I-girentuximab in the presurgical diagnosis of clear-cell renal cell cancer. Biologics 2012;6:395–407.
18. Krall N, Pretto F, Mattarella M, Müller C, Neri D. A technetium 99m-labeled ligand of carbonic anhydrase IX selectively targets renal cell carcinoma *in vivo*. J Nucl Med 2016;57:943–9.
19. Krall N, Pretto F, Neri D. A bivalent small molecule-drug conjugate directed against carbonic anhydrase IX can elicit complete tumour regression in mice. Chem Sci 2014;5:3640–4.
20. Krall N, Pretto F, Decurtins W, Bernardes GJL, Supuran CT, Neri D. A small-molecule drug conjugate for the treatment of carbonic anhydrase IX expressing tumors. Angew Chem Int Ed Engl 2014;53:4231–5.
21. Jain RK, Stylianopoulos T. Delivering nanomedicine to solid tumors. Nat Rev Clin Oncol 2010;7:653–64.
22. Yuan F, Dellian M, Fukumura D, Leunig M, Berk DA, Torchilin VP, et al. Vascular permeability in a human tumor xenograft: molecular size dependence and cutoff size. Cancer Res 1995;55:3752–6.
23. Leamon CP, Parker MA, Vlahov IR, Xu LC, Reddy JA, Vetzel M, et al. Synthesis and biological evaluation of EC20: a new folate-derived, ^{99m}Tc-based radiopharmaceutical. Bioconjugate Chem 2002;13:1200–10.
24. Müller C, Schibli R, Krenning EP, De Jong M. Pemetrexed improves tumor selectivity of ^{111}In-DTPA-folate in mice with folate receptor-positive ovarian cancer. J Nucl Med 2008;49:623–9.
25. Hillier SM, Maresca KP, Lu G, Merkin RD, Marquis JC, Zimmerman CN, et al. ^{99m}Tc-labeled small-molecule inhibitors of prostate-specific membrane antigen for molecular imaging of prostate cancer. J Nucl Med 2013;54:1369–76.
26. Ginj M, Zhang H, Waser B, Cescato R, Wild D, Wang X, et al. Radiolabeled somatostatin receptor antagonists are preferable to agonists for in vivo peptide receptor targeting of tumors. Proc Natl Acad Sci U S A 2006; 103:16436–41.
27. Wichert M, Krall N, Decurtins W, Franzini RM, Pretto F, Schneider P, et al. Dual-display of small molecules enables the discovery of ligand pairs and facilitates affinity maturation. Nat Chem 2015;7:241–9.
28. Gébleux R, Wulhfard S, Casi G, Neri D. Antibody format and drug release rate determine the therapeutic activity of noninternalizing antibody-drug conjugates. Mol Cancer Ther 2015;14:2606–12.
29. Perrino E, Steiner M, Krall N, Bernardes GJL, Pretto F, Casi G, et al. Curative properties of noninternalizing antibody-drug conjugates based on maytansinoids. Cancer Res 2014;74:2569–78.
30. Bernardes GJL, Casi G, Trüssel S, Hartmann I, Schwager K, Scheuermann J, et al. A traceless vascular-targeting antibody-drug conjugate for cancer therapy. Angew Chem Int Ed Engl 2012;51:941–4.
31. Du X, Beers R, Fitzgerald DJ, Pastan I. Differential cellular internalization of anti-CD19 and -CD22 immunotoxins results in different cytotoxic activity. Cancer Res 2008;68:6300–5.
32. Hilvo M, Baranauskiene L, Salzano AM, Scaloni A, Matulis D, Innocenti A, et al. Biochemical characterization of CA-IX, one of the most active carbonic anhydrase isozymes. J Biol Chem 2008;283:27799–809.
33. Pastorekova S, Parkkila S, Pastorek J, Supuran CT. Carbonic anhydrases: current state of the art, therapeutic applications and future prospects. J Enzyme Inhib Med Chem 2004;19:199–229.
34. Wichert M, Krall N. Targeting carbonic anhydrase IX with small organic ligands. Curr Opin Chem Biol 2015;26:48–54.
35. Divgi RC, Pandit-Taskar N, Jungbluth AA, Reuter VE, Gönen M, Ruan S, et al. Preoperative characterisation of clear-cell renal carcinoma using iodine-124-labelled antibody chimeric G250 (^{124}I-cG250) and PET in patients with renal masses: a phase I trial. Lancet Oncol 2007;8:304–10.
36. Bendell JC. An open-label Phase I dose-escalation study to evaluate the safety, tolerability, pharmacokinetics, and maximum tolerated dose of BAY 79–4620 in patients with advanced solid tumors. Bayer HealthCare Pharmaceuticals, Inc., USA; 2014 Jan. Report No.: PH-37705. Contract No.: NCT01028755.
37. McDonald PC, Winum JY, Supuran CT, Dedhar S. Recent developments in targeting carbonic anhydrase IX for cancer therapeutics. Oncotarget 2012; 3:84–97.
38. Tornøe CW, Christensen C, Meldal M. Peptidotriazoles on solid phase: [1,2,3]-triazoles by regiospecific copper(I)-catalyzed 1,3-dipolar cycloadditions of terminal alkynes to azides. J Org Chem 2002;67:3057–64.
39. Morris RT, Joyrich RN, Naumann RW, Shah NP, Maurer AH, Strauss HW, et al. Phase II study of treatment of advanced ovarian cancer with folate-receptor-targeted therapeutic (vintafolide) and companion SPECT-based imaging agent (99mTc-etarfolatide). Ann Oncol 2014;25:852–8.
40. Van Schaijk FG, Oosterwijk E, Molkenboer-Kuenen JD, Soede AC, McBride BJ, Goldenberg DM, et al. Pretargeting with bispecific anti-renal cell carcinoma x anti-DTPA(In) antibody in 3 RCC models. J Nucl Med 2005;46:495–501.
41. Dubowchik GM, Firestone RA, Padilla L, Willner D, Hofstead SJ, Mosure K, et al. Cathepsin B-labile dipeptide linkers for lysosomal release of doxorubicin from internalizing immunoconjugates: model studies of enzymatic drug release and antigen-specific *in vitro* anticancer activity. Bioconjug Chem 2002;13:855–69.
42. Choi KY, Swierczewska M, Lee S, Chen X. Protease-activated drug development. Theranostics 2012;2:156–78.
43. HogenEsch H, Nikitin AY. Challenges in pre-clinical testing of anti-cancer drugs in cell culture and in animal models. J Control Release 2012;164:183–6.
44. Martin K, Schreiner J, Zippelius A. Modulation of APC function and anti-tumor immunity by anti-cancer drugs. Front Immunol 2015;6:501.
45. Galluzzi L, Buqué A, Kepp O, Zitvogel L, Kroemer G. Immunological effects of conventional chemotherapy and targeted anticancer agents. Cancer Cell 2015;28:690–714.
46. Gutbrodt KL, Casi G, Neri D. Antibody-based delivery of IL2 and cytotoxics eradicates tumors in immunocompetent mice. Mol Cancer Ther 2014; 13:1772–6.
47. List T, Casi G, Neri D. A chemically defined trifunctional antibody-cytokine-drug conjugate with potent antitumor activity. Mol Cancer Ther 2014; 13:2641–52.
48. Lynch TJ, Bondarenko I, Luft A, Serwatowski P, Barlesi F, Chacko R, et al. Ipilimumab in combination with paclitaxel and carboplatin as first-line treatment in stage IIIB/IV non-small-cell lung cancer: results from a randomized, double-blind, multicenter phase II study. J Clin Oncol 2012;30:2046–54.